

# A STANDARD AND LINEAR FAN-BEAM FOURIER BACKPROJECTION THEOREM

PATRICIO GUERRERO\*, MATHEUS BERNARDI†, AND EDUARDO MIQUELES†

**ABSTRACT.** In this work we propose a theoretical low-complexity formulation for the tomographic fan-beam backprojection in standard and linear geometries. The proposed formula is obtained from a recent backprojection theorem in the parallel case. Such formula is written as a Bessel-Neumann series representation in the frequency domain in polar coordinates. A mathematical proof is provided together with numerical simulations compared with conventional fan-beam backprojection representations to validate our formulation showing more robustness when dealing with highly noisy data.

**Key words:** Fan-beam, backprojection, image reconstruction, Radon transform.

## 1. INTRODUCTION

Fan-beam tomographic measurements are used in different modalities of non-destructive imaging, as those obtained using X-rays. A typical tomographic device using fan-beam geometry is shown in Figure 1. This is a widely used and known technique, and there are many reconstruction algorithms for this configuration. After being generated with a given aperture angle and a fixed distance source-detector, the wavefront hits the sample originating a signal on the detector. Different propagation regimes can be considered with a varying distance [9, 11], although we will consider a pure mathematical signal idealized as the Radon transform of the given object.

For the tomographic parallel case by means of the classical backprojection formulation for image reconstruction, we can use the recently backprojection slice theorem formulation [12]. It is a formula that reduces a complete backprojection of a 2D sinogram from a computational cost of  $O(n^3)$  to  $O(n^2 \log n)$  with  $n \times n$  pixels in the final reconstructed image and  $n$  tomographic rotations. In this work, we want to take advantage of that formulation for two other popular fan-beam geometries, that are a) equispaced angles within the fan with a regular size  $\Delta\gamma$ , and b) equispaced points in a linear detector with a mesh step  $\Delta s$ . As indicated in [14], we refer to each acquisition as *standard fan* and *linear fan*, respectively, and illustrated at Figure 1.(a) and 1.(b). The linear case is easier to be implemented at a synchrotron beamline, whereas the first is more used with medical or industrial X-rays scans. For completeness, we discuss both the standard and the linear case.

---

\*MECHANICAL ENGINEERING DEPARTMENT, KU LEUVEN, 3001 LEUVEN, BELGIUM

†SCIENTIFIC COMPUTING GROUP, BRAZILIAN SYNCHROTRON LIGHT LABORATORY, NATIONAL CENTER FOR RESEARCH IN ENERGY AND MATERIALS, CAMPINAS, BRAZIL

Date: 7. October 2021.

Corresponding author: [patricio.guerrero@kuleuven.be](mailto:patricio.guerrero@kuleuven.be).

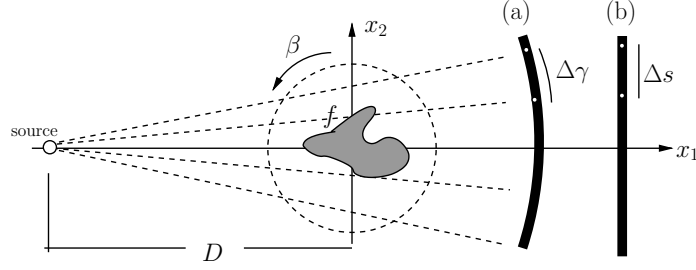


FIGURE 1. Tomographic setup for a fan-beam geometry: (a) *standard* detector, i.e., equispaced angular mesh with  $\Delta\gamma$ ; sinograms obtained here are denoted by  $w(\gamma, \beta)$  (b) *linear* detector, i.e., equispaced mesh at a perpendicular with the central ray and linear detector with  $\Delta s$ ; sinograms obtained here are denoted by  $g(s, \beta)$ .

In [20, 19] a generalized Fourier slice theorem for the case of fan-beam geometries is obtained, but presenting the same computational complexity as a conventional backprojection in the parallel case. Also, a strong rebinning process on the measured data is needed within the algorithm, which is not desirable in our case. Further relations on the frequency domain are obtained in [7] where a rebinning is also necessary. A more elegant approach is established in [2], but a rebinning in the frequency domain is also mandatory. Further advanced rebinning techniques are also established in [5] using a hierarchical approach. A series formulation where the backprojection is presented as the first order approximation for a general inversion in the standard fan-beam geometry is presented in [16].

This work is organized as follows. Chapter 2 presents a review of conventional fan-beam backprojections algorithms for both standard and linear geometries. In chapter 3 we rewrite the rebinning strategy in terms of the inverse rebinning operator as a two-step backprojection formula. Chapter 4 presents our fan-beam adjoint and backprojection theorems and its proof as a Bessel-Neumann series (referred here as BN series), representation in polar coordinates while chapter 5 supports numerically our method with simulated noisy data.

## 2. FAN-BEAM BACKPROJECTIONS

**2.1. The 2D Radon transform.** The two-dimensional Radon transform is defined as the linear operator  $\mathcal{R}: U \rightarrow V$  where  $U$  is the space of rapidly decreasing functions defined on  $\mathbb{R}^2$ , so-called *feature* space; and  $V$  is the *sinogram* space defined on the unit cylinder  $\mathbb{R} \times \mathbb{R}/2\pi\mathbb{Z}$  where  $\mathbb{R}/2\pi\mathbb{Z}$  is the quotient group of reals modulo  $2\pi$ . This definition holds when standard parallel projections are considered.

Let  $(t, \theta) \in \mathbb{R} \times \mathbb{R}/2\pi\mathbb{Z}$ , for  $f \in U$ ,  $\mathcal{R}f$  is defined as the integral

$$(1) \quad \mathcal{R}f(t, \theta) = \int_{\mathbb{R}^2} f(\mathbf{x}) \delta(t - \mathbf{x} \cdot \boldsymbol{\xi}_\theta) d\mathbf{x},$$

where  $\delta$  is the Delta distribution and  $\boldsymbol{\xi}_\theta = (\cos \theta, \sin \theta)^T$ . We will denote  $f_P \in U$  as a feature function acting on  $\mathbf{x} = (\rho, \phi) \in \mathbb{R}_+ \times [0, 2\pi[$  expressed in polar coordinates.  $\mathcal{R}f_P$  is then written as

$$(2) \quad \mathcal{R}f_P(t, \theta) = \int_0^{2\pi} \int_{\mathbb{R}_+} f_P(\rho, \phi) \delta(t - \rho \cos(\theta - \phi)) \rho d\rho d\phi.$$

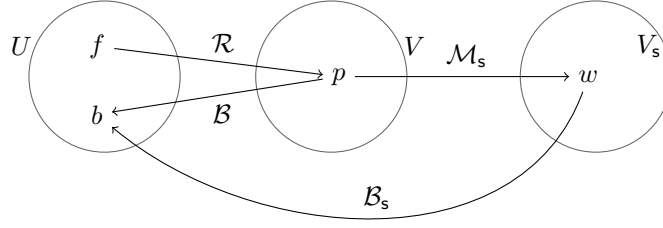


FIGURE 2. Action diagram for operators  $\{\mathcal{B}, \mathcal{R}\}$  and  $\{\mathcal{B}_s, \mathcal{R}_s\}$ , with  $\mathcal{R}_s = \mathcal{M}_s \mathcal{R}$ ,  $\mathcal{B}_s = \mathcal{B} \mathcal{M}_s^*$  and a generalized change of variables  $\mathcal{M}_s$ .

Note that  $\mathcal{R}f$  is an even function on the unit cylinder, that is,

$$(3) \quad \mathcal{R}f(t, \theta) = \mathcal{R}f(-t, \theta + \pi).$$

Adjoint and backprojection. Let  $T: X \rightarrow Y$  be a bounded linear operator between Hilbert spaces  $X$  and  $Y$ . Its adjoint operator is defined as the unique operator  $T^*: Y \rightarrow X$  that verifies

$$(4) \quad \forall u \in X, \quad \forall v \in Y, \quad \langle Tu, v \rangle_Y = \langle u, T^*v \rangle_X.$$

The adjoint and backprojection operators of the Radon transform [4] are closely related. The adjoint of  $\mathcal{R}$  is the operator  $\mathcal{R}^*: V \rightarrow U$  defined for  $p \in V$  and  $\mathbf{x} \in \mathbb{R}^2$  by

$$(5) \quad \mathcal{R}^*p(\mathbf{x}) = \int_0^{2\pi} p(\mathbf{x} \cdot \boldsymbol{\xi}_\theta, \theta) d\theta.$$

With standard  $L^2$  inner products on  $U$  and  $V$ , it is clear that  $\mathcal{R}^*$  verifies (4).

In the filtered backprojection (FBP) algorithm [14], the backprojection operation is applied after filtering the data with an adequate convolutional filter. Such backprojection operator, noted  $\mathcal{B}$  is defined by limiting last integral to  $[0, \pi]$ , and from the symmetry property (3) we have  $\mathcal{R}^* \equiv 2\mathcal{B}$ .

Computing  $\mathcal{B}p$  could be extremely expensive for discrete versions of the sinogram  $p$ , when  $\mathbf{x}$  covers a domain with a large number of points (pixels in practice) and also  $(t, \theta)$  covers a large number of pixels and a variety of angles (according to Crowther's criterion [3]). This is the case for synchrotron tomographic projections using high-resolution detectors with more than  $2048 \times 2048$  pixels and more than 2048 angles [13]. Recently [12], a low-complexity formulation for computing  $\mathcal{B}$  was obtained in the frequency domain using polar coordinates, the Backprojection Slice Theorem (BST). Such theorem reads for  $p \in V$  and  $\sigma > 0$ ,

$$(6) \quad \widehat{\mathcal{B}p}(\sigma \boldsymbol{\xi}_\theta) = \frac{\hat{p}(\sigma, \theta)}{\sigma},$$

where  $\widehat{\mathcal{B}p}$  is the 2D Fourier transform of  $\mathcal{B}p$  in polar frequency coordinates and  $\hat{p}$  the 1D Fourier transform of  $p$  with respect to  $t$ . The action of  $\{\mathcal{R}, \mathcal{B}\}$  is presented in Figure 2. It is a well known fact that  $\{p, f\}$  are related through the *Fourier slice Theorem* [14, 4], while  $\{b, p\}$  through the *backprojection slice theorem* [12].

**2.2. Fan-beam geometries.** There exist two different fan-beam parameterizations for the Radon transform [6], the first  $\mathcal{R}_s: U \rightarrow V_s$  is referred as the *standard fan-beam* transform, where the domain of sinograms  $V_s$  lies within the interval  $\mathbb{R}/\pi\mathbb{Z} \times \mathbb{R}/2\pi\mathbb{Z}$ . The second case,  $\mathcal{R}_\ell: U \rightarrow V_\ell$  is referred as the *linear fan-beam* transform, with sinograms domain  $V_\ell$  varying within the interval  $\mathbb{R} \times \mathbb{R}/2\pi\mathbb{Z}$ .

Let us consider  $(\gamma, \beta) \in \mathbb{R}/\pi\mathbb{Z} \times \mathbb{R}/2\pi\mathbb{Z}$  a pair of angles and  $s \in \mathbb{R}$ . Acting on a feature function  $f \in U$ , the linear operators  $\mathcal{R}_s$  and  $\mathcal{R}_\ell$  are defined respectively as

$$(7) \quad w(\gamma, \beta) = \mathcal{R}f(D \sin \gamma, \beta + \gamma),$$

and

$$(8) \quad g(s, \beta) = \mathcal{R}f\left(\frac{sD}{\sqrt{s^2 + D^2}}, \beta + \arctan \frac{s}{D}\right),$$

where  $D > 0$  is the distance of the focal point source to the origin, see Figure 1. Hence  $w \in V_s$  and  $g \in V_\ell$ . The following symmetry relationships holds,

$$(9) \quad \begin{aligned} w(\gamma, \beta) &= w(-\gamma, \beta + 2\gamma + \pi), \\ g(s, \beta) &= g(-s, \beta + 2 \arctan \frac{s}{D} + \pi). \end{aligned}$$

Since both operations represent a change of variables in the classical parallel sinogram, we can use the following notation,

$$(10) \quad \mathcal{R}_s f(\gamma, \beta) = \mathcal{M}_s \mathcal{R}f(\gamma, \beta), \quad \mathcal{R}_\ell f(s, \beta) = \mathcal{M}_\ell \mathcal{R}f(s, \beta),$$

where  $\mathcal{M}_s: V \rightarrow V_s$  and  $\mathcal{M}_\ell: V \rightarrow V_\ell$  are rebinning operators acting on a parallel sinogram  $p$ , respectively as

$$(11) \quad \begin{aligned} \mathcal{M}_s p(\gamma, \beta) &= p(D \sin \gamma, \beta + \gamma), \\ \mathcal{M}_\ell p(s, \beta) &= p\left(\frac{sD}{\sqrt{s^2 + D^2}}, \beta + \arctan \frac{s}{D}\right). \end{aligned}$$

From the experimental point of view, we assume that the origin is positioned at the center of rotation, where the sample is also centered. In both geometries, for simplicity and without any loss of generality, a 1D virtual detector will be considered centered at the origin. This can be done simply by scaling numerically the detector. In the standard geometry, the angle  $\gamma$  from the central ray indicates a position in the circle centered at the beam source with radius  $D$ , this circle acts as the detector in this geometry and then it's evidently  $2\pi$ -periodic on  $\gamma$ . Whereas in the linear geometry,  $s$  is the signed height on the linear detector perpendicular to the central ray and centered at the origin, see Figure 1.

The change of variables operation  $\mathcal{M}_s$  is depicted in Figure 2.  $\mathcal{M}_s$  and  $\mathcal{M}_\ell$  are well defined operators due to  $\beta + \gamma$  and  $\beta + \arctan \frac{s}{D}$  both belong to  $\mathbb{R}/2\pi\mathbb{Z}$ . Since is true that  $\mathcal{R}_s = \mathcal{M}_s \mathcal{R}$ , a conventional functional relation for space  $U$  and  $V_s$  provides us with the following statement,

$$(12) \quad \begin{aligned} \langle \mathcal{R}_s f, w \rangle_{V_s} &= \langle \mathcal{M}_s \mathcal{R}f, w \rangle_{V_s} \\ &= \langle \mathcal{R}f, \mathcal{M}_s^* w \rangle_V = \langle f, \mathcal{R}^* \mathcal{M}_s^* w \rangle_U. \end{aligned}$$

Therefore, it follows that  $\mathcal{R}_s^* = \mathcal{R}^* \mathcal{M}_s^*$ . In this work we propose a Fourier approach for equations

$$(13) \quad \mathcal{R}_s^* = \mathcal{R}^* \mathcal{M}_s^* \quad \text{and} \quad \mathcal{R}_\ell^* = \mathcal{R}^* \mathcal{M}_\ell^*.$$

**2.3. Integral representation of the adjoint transforms.** Considering both fan-beam geometries, we provide two main results for both the adjoint and back-projection operators of  $\mathcal{R}_s$  and  $\mathcal{R}_\ell$ . We denote in the following  $\mathbf{r}_\beta$  the Cartesian coordinates of the source.

**Lemma 1.** The operator  $\mathcal{R}_s^*: V_s \rightarrow U$ , defined for  $w \in V_s$  and  $\mathbf{x} \in \mathbb{R}^2$  by

$$(14) \quad \mathcal{R}_s^* w(\mathbf{x}) = \int_0^{2\pi} \frac{1}{L_\beta} w(\gamma_\beta, \beta) d\beta,$$

is the the adjoint of  $\mathcal{R}_s$  in the sense of (4). Here,  $L_\beta = \|\mathbf{r}_\beta - \mathbf{x}\|_2$  is the Euclidean distance of the source with the backprojected position  $\mathbf{x}$  and  $\gamma_\beta$  is the angle of such point within the fan, i.e.,  $\cos \gamma_\beta = \frac{1}{DL_\beta} \mathbf{r}_\beta \cdot (\mathbf{r}_\beta - \mathbf{x})$ .

*Proof.* Let  $f_P \in U$  and  $w \in V_s$ . Using the polar representation (2) of  $\mathcal{R}$  and the relationship  $\rho \cos(\beta + \gamma - \phi) = L_\beta \sin(\gamma_\beta - \gamma)$  [6], then

$$(15) \quad \begin{aligned} \langle \mathcal{R}_s f_P, w \rangle_{V_s} &= \int_0^{2\pi} \int_0^\pi w(\gamma, \beta) \mathcal{R}_s f_P(\gamma, \beta) d\gamma d\beta \\ &= \int_0^{2\pi} \int_0^\pi w(\gamma, \beta) \int_0^{2\pi} \int_{\mathbb{R}_+} f_P(\rho, \phi) \delta(L_\beta \sin(\gamma_\beta - \gamma)) \rho d\rho d\phi d\gamma d\beta, \end{aligned}$$

which, from Fubini's theorem, becomes

$$\langle \mathcal{R}_s f_P, w \rangle_{V_s} = \int_0^{2\pi} \int_{\mathbb{R}_+} f(\rho, \phi) \int_0^{2\pi} \int_0^\pi \frac{1}{L_\beta} w(\gamma, \beta) \delta(\sin(\gamma_\beta - \gamma)) d\gamma d\beta \rho d\rho d\phi.$$

Therefore, since  $\delta(\sin(\gamma_\beta - \gamma)) = \delta(\gamma_\beta - \gamma)$  for  $\gamma \in [0, \pi[$  and a fixed  $\gamma_\beta$ , after performing the above  $\gamma$ -integration,  $\mathcal{R}_s^*$  defined in (14) verifies (4).  $\square$

**Lemma 2.** The operator  $\mathcal{R}_\ell^*: V_\ell \rightarrow U$ , defined for  $g \in V_\ell$  and  $\mathbf{x} \in \mathbb{R}^2$  by

$$(16) \quad \mathcal{R}_\ell^* g(\mathbf{x}) = \frac{1}{D} \int_0^{2\pi} \frac{1}{U_\beta} \sqrt{s_\beta^2 + D^2} g(s_\beta, \beta) d\beta,$$

is the adjoint of  $\mathcal{R}_\ell$  in the sense of (4).  $U_\beta$  is the ratio of the scalar projection of  $\mathbf{r}_\beta - \mathbf{x}$  on the central ray to the source-origin distance, and  $s_\beta$  is the corresponding height  $s$  for  $\mathbf{x}$  at a source angle  $\beta$ , i.e.,

$$(17) \quad U_\beta = \frac{D^2 - \mathbf{r}_\beta \cdot \mathbf{x}}{D^2}, \quad s_\beta = \frac{\mathbf{x} \cdot \boldsymbol{\xi}_\beta}{U_\beta}.$$

*Proof.* As the proof of Lemma 1, it follows directly from (4) and the polar representation (2).  $\square$

It is worth to mention the relation between the adjoint transforms in (14) and (16) and the backprojection operators, noted here  $\mathcal{B}_s$  and  $\mathcal{B}_\ell$  respectively for the standard and linear geometry. The backprojection operators are applied on the FBP algorithm as in the parallel case after the filtering process [6]. Such operators are respectively defined as the weighted integrals

$$(18) \quad \mathcal{B}_s w(\mathbf{x}) = \int_0^{2\pi} \frac{1}{L_\beta^2} w(\gamma_\beta, \beta) d\beta, \quad \mathcal{B}_\ell g(\mathbf{x}) = \int_0^{2\pi} \frac{1}{U_\beta^2} g(s_\beta, \beta) d\beta,$$

therefore, the difference with the adjoint transforms lies on the weight factors.

## 3. TWO-STEP BACKPROJECTION FORMULAS

The two-step adjoint formulations for each geometry, namely  $\mathcal{R}_s^* = \mathcal{R}^* \mathcal{M}_s^*$  and  $\mathcal{R}_\ell^* = \mathcal{R}^* \mathcal{M}_\ell^*$  derived following (12) are going to be detailed here. It is clear that the adjoint of the rebinning operators  $\{\mathcal{M}_s, \mathcal{M}_\ell\}$  plays an important role in such formulations.

**Lemma 3** (Adjoint of a rebinning operator). Let  $\mathcal{M} : X \rightarrow Y$  be a bijective and differentiable with continuous inverse rebinning operator between two Hilbert spaces  $X$  and  $Y$ . Its adjoint  $\mathcal{M}^* : Y \rightarrow X$  is then given by  $\mathcal{M}^* = \mathbf{J} \mathcal{M}^{-1}$ , where  $\mathbf{J}$  is the Jacobian determinant of the rebinning operation and  $\mathcal{M}^{-1}$  its inverse rebinning.

*Proof.* If  $u \in X$  and  $v \in Y$ , a direct verification of  $\langle \mathcal{M}u, v \rangle_Y = \langle u, \mathcal{M}^*v \rangle_X$  through an integral representation and a change of variables will prove the result. Bijectivity of  $\mathcal{M}$  is needed to preserve the range of integration in both domains of  $X$  and  $Y$  and for the inverse to exist.  $\square$

**Lemma 4.** The adjoint operator of  $\mathcal{M}_s$  and  $\mathcal{M}_\ell$  are respectively defined for  $w \in V_s$  and  $g \in V_\ell$  by

$$(19) \quad \mathcal{M}_s^* w(t, \theta) = w(\gamma(t), \theta - \gamma(t)) \mathbf{J}_s(t),$$

$$(20) \quad \mathcal{M}_\ell^* g(t, \theta) = g(s(t), \theta - \gamma(t)) \mathbf{J}_\ell(t),$$

where

$$(21) \quad \gamma(t) = \arcsin \frac{t}{D}, \quad s(t) = \frac{tD}{\sqrt{D^2 - t^2}}, \quad \mathbf{J}_s(t) = \frac{1}{\sqrt{D^2 - t^2}}, \quad \mathbf{J}_\ell(t) = \frac{D^3}{(D^2 - t^2)^{3/2}}.$$

*Proof.* As both operators are bijective [14] and continuously differentiable, this is an immediate application of Lemma 3.  $\square$

The formal adjoints of  $\mathcal{R}_s$  and  $\mathcal{R}_\ell$  are presented in Lemmas 1 and 2. The problem with these formulations is the difficulty for a low-cost implementation algorithm. To circumvent this problem, we use the fact that  $\{\mathcal{R}, \mathcal{R}^*\}$  are bounded operators between Hilbert spaces  $U$  and  $V$ , here understood as the space of rapidly decreasing functions. Hence, we obtain the following result.

**Theorem 1.** *Considering the two fan-beam geometries, formal adjoints for operators  $\mathcal{R}_s$  and  $\mathcal{R}_\ell$  are given explicitly by expressions (14) and (16), which on the other hand, are also given by  $\mathcal{R}_s^* = \mathcal{R}^* \mathcal{M}_s^*$  and  $\mathcal{R}_\ell^* = \mathcal{R}^* \mathcal{M}_\ell^*$  respectively.*

*Proof.* This is an immediate consequence of the uniqueness of the adjoint for bounded operators on Hilbert spaces. In fact, since  $\mathcal{R}^*$  and  $\mathcal{M}_s^*$  are bounded, the composition is also bounded. The same applies for  $\mathcal{M}_\ell^*$ .  $\square$

It is also worth to provide a straightforward two-step rebinning formulation for the backprojection operators as  $\mathcal{B}_s = \mathcal{B} \mathcal{M}_s^{-1}$  and  $\mathcal{B}_\ell = \mathcal{B} \mathcal{M}_\ell^{-1}$  having an evident justification. The difference mainly lies on the Jacobian determinants  $\mathbf{J}_s$  and  $\mathbf{J}_\ell$ .

## 4. MAIN BACKPROJECTION THEOREMS

**4.1. Standard geometry.** The main result of this work is based on a Fourier approach for equations (13) and then make use of the BST formula (6) and the identity  $\mathcal{R}^* \equiv 2\mathcal{B}$  for a fixed  $\theta$  and  $\sigma > 0$  in the form

$$(22) \quad \widehat{\mathcal{R}_s^* w}(\sigma \xi_\theta) = \widehat{\mathcal{R}^* \mathcal{M}_s^* w}(\sigma, \theta) = \frac{2}{\sigma} \widehat{\mathcal{M}_s^* w}(\sigma, \theta).$$

We start announcing our Fourier-based fan-beam backprojection theorem for standard geometry, and then we show how it is easily adapted to the linear case. From (22), we observe the need of computing  $\widehat{\mathcal{M}_s^* w}$  that is written as a series representation in the following Lemma.

**Lemma 5.** Given a standard fan-beam sinogram  $w \in V_s$ , first define  $z \in V_s$  by  $z(\gamma, \theta) = w(\gamma, \theta - \gamma)$  for all  $(\gamma, \theta) \in \mathbb{R}/\pi\mathbb{Z} \times \mathbb{R}/2\pi\mathbb{Z}$ . As  $z$  is  $2\pi$ -periodic with respect to  $\gamma$  we can write its Fourier series expansion with the Fourier coefficients

$$(23) \quad c_n(\theta) = \frac{1}{2\pi} \int_0^{2\pi} z(\gamma, \theta) e^{-in\gamma} d\gamma,$$

from where we define the coefficients

$$(24) \quad b_n = 2\pi[c_n + (-1)^n \bar{c}_n] \quad \text{for } n \geq 1, \quad \text{and} \quad b_0 = 2\pi c_0.$$

Then we have a BN series description of  $\widehat{\mathcal{M}_s^* w}$  as

$$(25) \quad \widehat{\mathcal{M}_s^* w}(\sigma, \theta) = \sum_{n=0}^{\infty} b_n(\theta) J_n(D\sigma),$$

where  $(J_n)$  is a sequence of Bessel functions of the first kind.

*Proof.* Given  $w \in V_s$ , from (19) and (21) the 1D Fourier transform of  $\mathcal{M}_s^* w(t, \theta)$  with respect to  $t$  is

$$(26) \quad \begin{aligned} \widehat{\mathcal{M}_s^* w}(\sigma, \theta) &= \int_{\mathbb{R}} w(\gamma(t), \theta - \gamma(t)) e^{-it\sigma} J_s(t) dt \\ &= \int_0^{2\pi} w(\gamma, \theta - \gamma) e^{-iD\sigma \sin \gamma} d\gamma = \int_0^{2\pi} z(\gamma, \theta) e^{-iD\sigma \sin \gamma} d\gamma. \end{aligned}$$

After expanding  $Z$  with  $c_n$  we have

$$(27) \quad \begin{aligned} \widehat{\mathcal{M}_s^* w}(\sigma, \theta) &= \sum_n c_n(\theta) \int_0^{2\pi} e^{i[n\gamma - D\sigma \sin \gamma]} d\gamma \\ &= 2\pi \sum_n c_n(\theta) J_n(D\sigma), \end{aligned}$$

from where the result claims using (24) and the property  $J_{-n}(x) = (-1)^n J_n(x)$ .  $\square$

We can now state our fan-beam backprojection theorem for standard geometries.

**Theorem 2** (Standard fan-beam adjoint Theorem). *The adjoint operator  $\mathcal{R}_s^*: V_s \rightarrow U$  acting on  $w \in V_s$  can be written in the Fourier domain as the series*

$$(28) \quad \widehat{\mathcal{R}_s^* w}(\sigma \xi_\theta) = \frac{2}{\sigma} \sum_{n=0}^{\infty} b_n(\theta) J_n(D\sigma),$$

where  $(\sigma, \theta) \in \mathbb{R}_+ \times \mathbb{R}/2\pi\mathbb{Z}$  and the coefficients  $b_n$  are computed as in Lemma 5.

*Proof.* This is an immediate consequence of (22) and Lemma 5.  $\square$

**Remark 1.** For direct FBP numerical implementation interests, the backprojection operator  $\mathcal{B}_s$  is also writable as a BN series. From  $\mathcal{B}_s = \mathcal{B}\mathcal{M}_s^{-1}$  we have

$$(29) \quad \widehat{\mathcal{B}_s w}(\sigma \xi_\theta) = \widehat{\mathcal{B}\mathcal{M}_s^{-1} w}(\sigma, \theta) = \frac{1}{\sigma} \widehat{\mathcal{M}_s^{-1} w}(\sigma, \theta).$$

Then, the Jacobian determinant  $J_s$  in the derivation (26) needs to be compensated. Due to  $dt = D \cos \gamma d\gamma$  in (26), we define  $\dot{z} = \mathcal{A}w$  by

$$(30) \quad \mathcal{A}w(\gamma, \theta) = D \cos \gamma w(\gamma, \theta - \gamma),$$

and then we compute the Fourier coefficients  $(\dot{b}_n)$  from  $\dot{z}$  in the same way as in (24). Following the same derivation of Theorem 2, we have the representation

$$(31) \quad \widehat{\mathcal{B}_s w}(\sigma \xi_\theta) = \frac{1}{\sigma} \sum_{n=0}^{\infty} \dot{b}_n(\theta) J_n(D\sigma).$$

Moreover, from the rebinning operation  $\beta = \theta - \gamma$  we note that to perform the backprojection with the BN series, we only need a short-scan sinogram where  $\beta \in [0, \pi + 2\bar{\gamma}]$ , with  $\bar{\gamma} = \arcsin \bar{x}/D$  the upper bound of  $\gamma$  such that the beam intersects the domain of the phantom bounded by  $\|\mathbf{x}\|_2 \leq \bar{x}$ .

**Remark 2.** The backprojected image obtained with BN series (31) assumes a null DC component due to the kernel  $1/\sigma$ . However, (31) can still be used to reconstruct an arbitrary object  $f$  with the correct DC component  $\kappa$  by estimating it using the volume conservation property of the Radon transform [14] that states

$$(32) \quad \kappa = \int_{\mathbb{R}^2} f(\mathbf{x}) d\mathbf{x} = \int_{\mathbb{R}} \mathcal{R}f(t, \theta) dt, \quad \forall \theta.$$

Then, using the rebinning operator  $\mathcal{M}_s$ ,  $\kappa$  can be estimated from fan-beam projections  $\mathcal{R}_s f$  by

$$(33) \quad \kappa = \int_{\mathbb{R}} \mathcal{R}f(t, \theta) dt = \int_{\mathbb{R}} \mathcal{M}_s^{-1} \mathcal{R}_s f(t, \theta) dt, \quad \forall \theta;$$

averaging last integral over  $\theta$  is also possible when having noisy projections.

**Remark 3.** Convergence of the BN series (31) is guaranteed due to the fact that  $J_n(x)$  has a pointwise convergence to 0 since  $|J_n(x)| \leq |\frac{1}{2}x|^n/n!$  for all  $x \in \mathbb{R}_+$  [1, eq. 9.1.62].

**4.2. Linear geometry.** The adjoint operator for the linear fan-beam transform follows. Switching between fan-beam geometries requires only a one-dimensional interpolation on the first variable. In fact, taking  $g \in V_\ell$ , the rebinning operator on the first variable  $\mathcal{L}: V_\ell \rightarrow V_s$  is defined by

$$(34) \quad \mathcal{L}g(\gamma, \beta) = \begin{cases} g(D \tan \gamma, \beta), & \text{if } \gamma \neq \pi/2 \pmod{\pi} \\ 0, & \text{otherwise} \end{cases} \iff \mathcal{R}_s = \mathcal{L}\mathcal{R}_\ell.$$

provides a sinogram  $w$  on the space  $V_s$ . Such bijective operator, according to Lemma 3, has an adjoint operator given by

$$(35) \quad \mathcal{L}^* w(s, \beta) = J(s) \mathcal{L}^{-1} w(s, \beta),$$

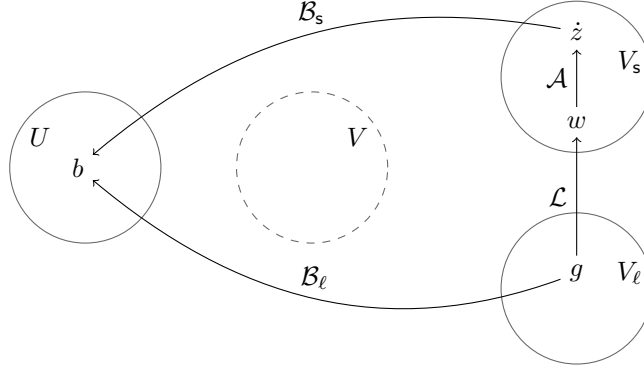


FIGURE 3. Diagram for the backprojection operators  $\{\mathcal{B}_s, \mathcal{B}_\ell\}$  (without rebinning to the space  $V$ ) through the action of operators  $\{\mathcal{L}, \mathcal{A}\}$ . See text for details

where

$$(36) \quad J(s) = \frac{D}{D^2 + s^2}, \quad \mathcal{L}^{-1}w(s, \beta) = w(\arctan \frac{s}{D}, \beta).$$

The following Theorem enables us to provide a backprojection algorithm for the linear fan-beam geometry.

**Theorem 3.** *The adjoint operators  $\mathcal{R}_s^*$  and  $\mathcal{R}_\ell^*$  are related, for all  $g \in V_\ell$  by*

$$(37) \quad \mathcal{R}_\ell^* g = \mathcal{R}_s^* \tau \mathcal{L} g,$$

where  $\tau(\gamma) = D \sec^2 \gamma$ .

*Proof.* From (34) we obtain  $\mathcal{R}_s^* = (\mathcal{L} \mathcal{R}_\ell)^* = \mathcal{R}_\ell^* \mathcal{L}^*$ , from where follows  $\mathcal{R}_\ell^* = \mathcal{R}_s^* (\mathcal{L}^*)^{-1}$ . Using (35) and the fact that  $(\mathcal{L}^*)^{-1} = J(s(\gamma))^{-1} \mathcal{L}$  with  $s(\gamma) = D \tan \gamma$ , equation (37) is obtained.  $\square$

Therefore, our resulting formulation for the linear fan-beam adjoint transform is obtained by the following construction.

**Theorem 4** (Linear fan-beam adjoint Theorem). *The operator  $\mathcal{R}_\ell^*: V_s \rightarrow U$  acts on  $g \in V_\ell$  as the following two-steps operation.*

- (i) *Let  $\dot{w}(\gamma, \beta) = \tau(\gamma)w(\gamma, \beta)$  with  $w = \mathcal{L}g$  be in  $V_s$ .*
- (ii) *The adjoint operator is obtained as the BN series (28) where the coefficients  $(b_n)$  in (24) are obtained from  $\dot{z}(\gamma, \theta) = \dot{w}(\gamma, \theta - \gamma)$ .*

*Proof.* Each step is justified respectively by Theorems 3 and 2.  $\square$

Finally, the backprojection operator  $\mathcal{B}_\ell$  can also be computed in the same way as in Remark 1, by first writing  $\mathcal{B}_\ell g = \mathcal{B}_s \mathcal{L} g$  and then computing  $\mathcal{B}_s$  using (31).

Figure 3 illustrates the action of our method, where a backprojection  $b \in U$  is obtained in two-steps. The unknown backprojection  $\mathcal{B}_\ell g$  is obtained in the frequency domain from (28), using polar coordinates by two main operations to obtain sinogram  $\dot{z} \in V_s$  through  $\mathcal{L}$  defined in (34) (interpolation on the first variable) and  $\mathcal{A}$  defined in (30) (interpolating on the second variable).

**Remark 4** (Passage to Cartesian coordinates). A backprojected fan-beam sinogram using Theorems 2 or 4 is obtained in polar coordinates  $(\sigma, \theta) \in \mathbb{R}_+ \times \mathbb{R}/2\pi\mathbb{Z}$  that needs to be mapped into Cartesian coordinates before applying the inverse Fourier transform. This problem is also present in parallel geometry if using the Fourier reconstruction method based on the Fourier Slice theorem [14] or using the BST approach [12]. The evident solution is a straightforward (linear) interpolation with the expense of important errors at higher frequencies. A gridding strategy [14] can also be used by weighting the polar data with an adequate function and then the mapping to Cartesian is performed by convolution with such weigh function. This method is proven to handle better interpolations errors [10]. Another strategy is to iteratively regularize the passage to Cartesian coordinates using Total Variation regularization based on the approach developped on [18] in the parallel setting.

## 5. NUMERICAL RESULTS

Simulations are concentrated on the linear case due to the standard case is one rebinning operation less than the linear, so results would be slightly better. The Shepp-Logan phantom in Figure 4(a) is considered. We first computed the parallel Radon transform (1) to then obtain a linear fan sinogram through operation  $\mathcal{M}_\ell$  (11).

Discrete configuration. The domain of the feature phantom is the unit disk  $\|\mathbf{x}\|_2 \leq 1$  where we have a  $N \times N$  uniformly sampled quadrilateral mesh domain. For the domain of  $U$  to compute (1), we have  $N \times N_\theta$  points uniformly spaced with  $(t, \theta) \in [-1, 1] \times [0, \pi]$ .

For the linear fan-beam geometry, we consider the distance source-origin  $D = 8$ , then  $\bar{s} = D(D^2 - 1)^{-1/2}$  is the highest detector position that measures the sample on the unit disk subtending an angle  $\bar{\gamma} = \arcsin 1/D$ . We recall that the detector is supposed to be centred, or scaled, at the origin. Due to the symmetry property (9) and to Remark 1,  $(s, \beta)$  needs to cover the sets  $[-\bar{s}, \bar{s}] \times [0, \pi + 2\bar{\gamma}[$ . For simplicity, we sampled these sets as in the parallel geometry uniformly with  $N$  and  $N_\theta$  points. Finally, here we will use  $N = N_\theta = 512$ .

Implementation and complexity. Implementation details of the two steps of Theorem 4 follows. Step (i) is a sequence of two 1D interpolations,  $\mathcal{L}$  followed by  $\mathcal{A}$  to obtain  $\dot{z}$ .  $\mathcal{L}$  is a rebinning on the spatial variable from linear to standard geometry, so only needed in the linear case, and  $\mathcal{A}$  is a linear operation on the angular variable then not causing strong rebinning errors with linear interpolation. More importantly, both operations are not expensive having complexity  $O(NN_\theta)$  and they were easily parallelized as they are both one-dimensional.

Step (ii) is more challenging, we need to compute a truncated BN series (31) until convergence. Of course the number of terms in the sequence  $\{J_n\}$  is the same of  $\{b_n\}$ , that itself is the number of samples of  $s$  in the sinogram  $g$  following the Nyquist sampling theorem [6]. Convergence of the series can thus be reached by first zero-padding the linear variable  $s$  of  $g$ , or equivalently,  $\gamma$  of  $\dot{z}$  after performing operation  $\mathcal{A}$ .

Computing coefficients  $\{b_n\}$  requires  $N_\theta$  independent 1D Fourier transforms to obtain (23) followed by the easy operation (24). They were also parallelized in  $\theta$  having a complexity  $O(N \log N)$  each with Fast Fourier techniques. Importantly, the sequence  $\{J_n(D\sigma)\}$  in (31) not depending on the sample is computed only once

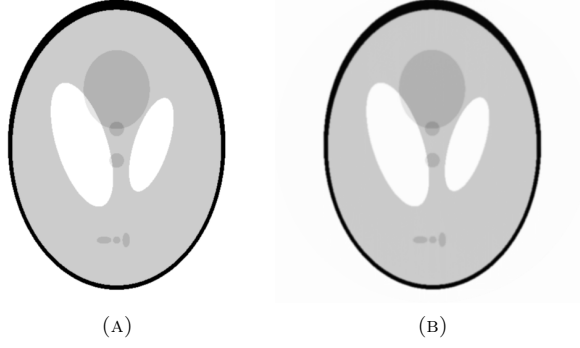


FIGURE 4. Feature phantom (a) and reconstruction (b) using the BN series of Theorem 4.

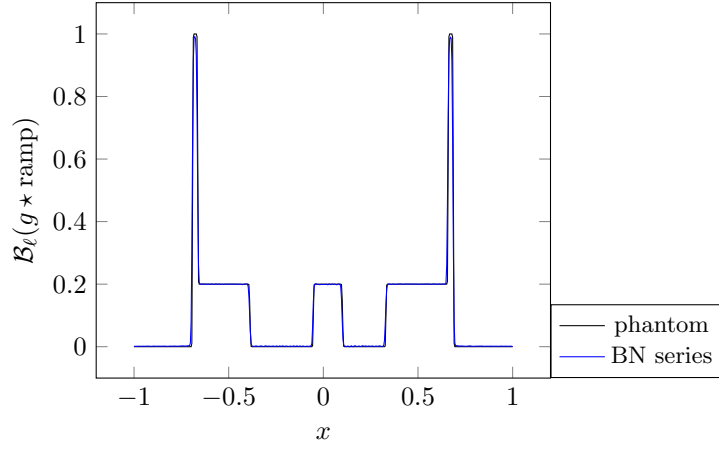
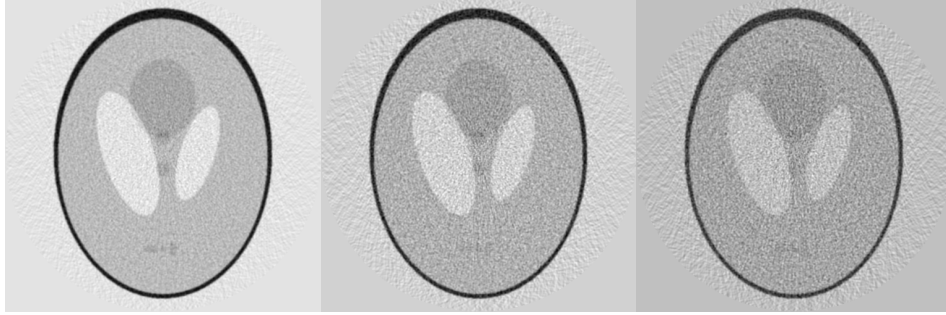


FIGURE 5. Middle profiles ( $y = 0$ ) of the Shepp-Logan phantom and the reconstruction through FBP by our BN series method.

for a given setup and can be used as a *lookup table* for the computation of (31), not being costly at computing time.

After truncating sum (31), computing it results simply on a matrix multiplication of the matrices composed with elements  $\{\dot{b}_n(\theta)\}$  and  $\{J_n(D\sigma)\}$  for sampled values of  $\{\theta, \sigma\}$ . The frequency variable  $\sigma$  was sampled following the Nyquist sampling theorem. Such multiplication has a complexity of  $O(N^3)$  but can be reduced to  $O(N^{2.3729})$  with fast matrix multiplication algorithms [8, 17], although we used the direct approach in our simulations. We recall that conventional approaches present a cost of  $O(N^3)$ . Even using a conventional  $O(N^3)$  matrix multiplication algorithm, the simplicity and straightforward parallel implementation of matrix multiplication related to a standard backprojection algorithm makes this approach still interesting. Finally, the Fourier domain of the backprojected image is obtained at a polar grid followed by linear interpolation to Cartesian coordinates and the 2D inverse (fast) Fourier Transform, operations with respective complexity of  $O(N^2)$  and  $O(N^2 \log N)$ .

BN series



Rebinning

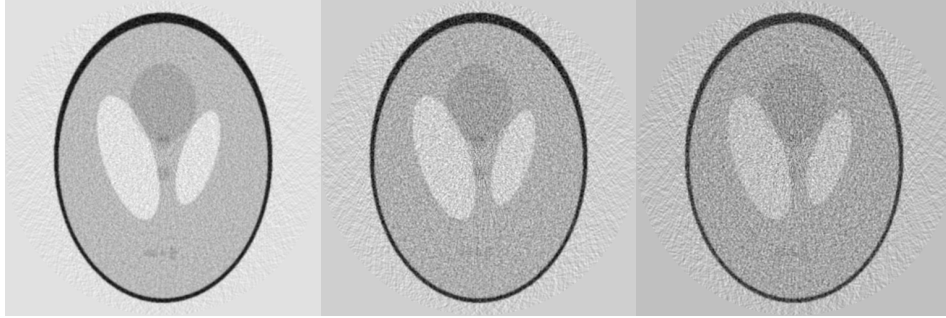
Sinogram  
MSE: 0.5Sinogram  
MSE: 2Sinogram  
MSE: 4

FIGURE 6. Reconstructions using the BN series (first row) and rebinning (second row) with equally increasing sinogram Poisson noise.

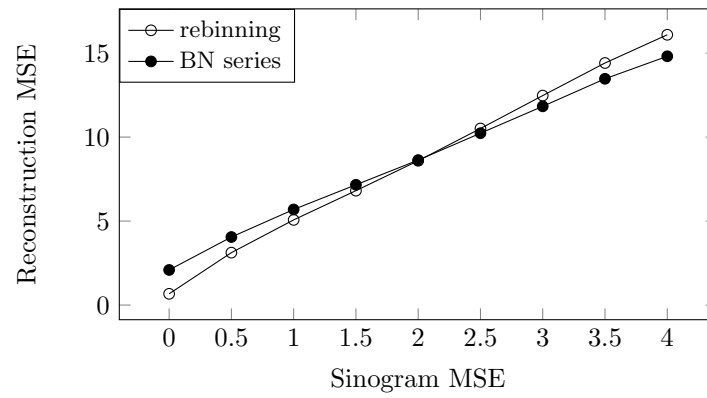


FIGURE 7. Reconstruction MSE vs sinogram MSE. Both methods have linear behavior but the BN series with a weaker slope than the rebinning method.

Both algorithms were implemented on a multithreading architecture for each step. We used the numerical library `scipy` [15] to compute Fast Fourier transforms, linear interpolations and Bessel coefficients. Although the theoretical interest of our formula (31) is the main goal of this work, computing time can be reduced with optimized codes related to conventional backprojections because of the lower computational complexity, when fully exploiting fast matrix multiplication and fast Fourier transform algorithms.

Reconstruction results. To obtain image reconstructions, we filtered the parallel sinogram with the conventional ramp filter [6] before applying the rebinning operation  $\mathcal{M}_\ell$  to obtain a filtered fan-beam sinogram. We proceeded in this way for sake of simplicity because the filtering processes for fan-beam sinograms, detailed in [6, 14], is not in the scope of this work but only the backprojection operation.

The normalised mean square error (MSE) computed as  $100 \left\| f - \tilde{f} \right\|_2^2 \left\| f \right\|_2^{-2}$  for a ground truth image  $f$  and corrupted  $\tilde{f}$  is used as the error metric.

Two backprojections methods were implemented, the conventional rebinning through parallel geometry by operation  $\mathcal{M}_\ell^{-1}$  in (20) followed by the standard  $O(N^2 \log N)$  backprojection  $\mathcal{B}$  as presented in theorem 1 and our BN series method. With noiseless data almost perfect reconstructions were obtained with the rebinning method (not shown) mainly due to the sinogram was obtained through  $\mathcal{M}_\ell$ . With the BN series the results are also almost exact, showed in Figure 4(b) and the associated middle ( $y = 0$ ) profile in Figure 5. Reconstruction MSE is still better with the rebinning method with noiseless data, see the noiseless data reconstruction MSE for nul sinogram MSE in Figure 7.

Then, we added Poisson noise to sinograms with increasing MSE, images are shown in Figure 6 with no visual difference between both methods. However, as the noise increases, BN series method behaves better as shown in Figure 6 where both reconstruction MSE appears to grow linearly with noise but the BN series with a weaker slope. This could be due to the effect of 2D interpolations of operator  $\mathcal{M}_\ell^{-1}$  on noisy sinograms.

## 6. CONCLUSIONS

We have proposed in this work a backprojection formulation for fan-beam scanning with standard and linear detectors. The linear case being more interesting in synchrotron context was developed as a two-step process. The first step consists on a sequence of simple one-dimensional operators where a standard fan-beam sinogram is obtained. The second step, the backprojection operation, is performed by writing the Fourier transform of the backprojected image as a Bessel-Neumann series on the frequency variable  $\sigma$  weighted by  $1/\sigma$ . The coefficients of the expansion are in fact the Fourier coefficients of the sinogram obtained in the first step. This approach, based on the low cost backprojection BST formula [12] for parallel sinograms, presents a reduction on the computational cost related to conventional fan-beam backprojections when fast matrix multiplication and fast Fourier transforms algorithms are used, and a simpler formulation as a two-matrix multiplication. Iterative reconstruction algorithms where the backprojection process is computed on each iteration, as the EM algorithm [14] can also take advantage of this formulation to obtain robust reconstructions. A second interesting feature is the absence of a strong rebinning process from fan to parallel beam projections as is mostly done in

other fan-backprojection algorithms. This results on better handling of noisy data where interpolations can have strong negative effects as shown in our numerical simulations when increasing linearly the noise level and our method over-perform the rebinning strategy. When dealing with standard fan-beam data, the first step of the algorithm is more straightforward where only one linear change of variables is needed without lying on interpolations errors.

## REFERENCES

- [1] M. Abramowitz and I. A. Stegun, editors. *Handbook of Mathematical Functions with Formulas, Graphs, and Mathematical Tables*. National Bureau of Standards, 1964.
- [2] G.-H. Chen, S. Leng, and C. A. Mistretta. A novel extension of the parallel-beam projection-slice theorem to divergent fan-beam and cone-beam projections. *Medical physics*, 32(3):654–665, 2005.
- [3] R. A. Crowther, D. DeRosier, and A. Klug. The reconstruction of a three-dimensional structure from projections and its application to electron microscopy. *Proc. R. Soc. Lond. A*, 317(1530):319–340, 1970.
- [4] S. R. Deans. *The Radon transform and some of its applications*. Courier Corporation, 2007.
- [5] A. George and Y. Bresler. A fast fan-beam backprojection algorithm based on efficient sampling. *Physics in Medicine & Biology*, 58(5):1415, 2013.
- [6] A. C. Kak and M. Slaney. *Principles of computerized tomographic imaging*. Society for Industrial and Applied Mathematics, 2001.
- [7] D. Kazantsev and V. Pickalov. Fan-beam tomography iterative algorithm based on fourier transform. In *Nuclear Science Symposium Conference Record, 2008. NSS'08. IEEE*, pages 4138–4139, 2008.
- [8] F. Le Gall. Powers of tensors and fast matrix multiplication. In *Proceedings of the 39th International Symposium on Symbolic and Algebraic Computation*, ISSAC '14, page 296–303, New York, NY, USA, 2014. Association for Computing Machinery.
- [9] D. R. Luke, J. V. Burke, and R. G. Lyon. Optical wavefront reconstruction: Theory and numerical methods. *SIAM review*, 44(2):169–224, 2002.
- [10] F. Marone and M. Stampanoni. Regridding reconstruction algorithm for real-time tomographic imaging. *Journal of synchrotron radiation*, 19(6):1029–1037, 2012.
- [11] E. Miqueles and P. Guerrero. Automatic regularization for tomographic image reconstruction. *Results in Applied Mathematics*, 6:100088, 2020.
- [12] E. Miqueles, N. Koshev, and E. S. Helou. A backprojection slice theorem for tomographic reconstruction. *IEEE Transactions on Image Processing*, 27(2):894–906, 2018.
- [13] E. Miqueles, G. Martinez Jr., and P. Guerrero. Fast image reconstruction at a synchrotron laboratory. In *Proceedings of the 2020 SIAM Conference on Parallel Processing for Scientific Computing*, pages 24–34, 2020.
- [14] F. Natterer and F. Wübbeling. *Mathematical methods in image reconstruction*, volume 5. Siam, 2001.
- [15] P. Virtanen, R. Gommers, T. E. Oliphant, M. Haberland, T. Reddy, D. Cournapeau, E. Burovski, P. Peterson, W. Weckesser, J. Bright, S. J. van der Walt, M. Brett, J. Wilson, K. Jarrod Millman, N. Mayorov, A. R. J. Nelson, E. Jones, R. Kern, E. Larson, C. Carey, Í. Polat, Y. Feng, E. W. Moore, J. Vand erPlas, D. Laxalde, J. Perktold, R. Cimrman, I. Henriksen, E. A. Quintero, C. R. Harris, A. M. Archibald, A. H. Ribeiro, F. Pedregosa, P. van Mulbregt, and S. . Contributors. SciPy 1.0: Fundamental Algorithms for Scientific Computing in Python. *Nature Methods*, 2020.
- [16] Y. Wei, G. Wang, and J. Hsieh. Relation between the filtered backprojection algorithm and the backprojection algorithm in ct. *IEEE Signal Processing Letters*, 12(9):633–636, 2005.
- [17] V. V. Williams. Multiplying matrices faster than coppersmith-winograd. In *Proceedings of the forty-fourth annual ACM symposium on Theory of computing*, pages 887–898, 2012.
- [18] X.-Q. Zhang and J. Froment. Total variation based fourier reconstruction and regularization for computer tomography. In *IEEE Nuclear Science Symposium Conference Record, 2005*, volume 4, pages 2332–2336, 2005.
- [19] S. Zhao, K. Yang, and K. Yang. Fan beam image reconstruction with generalized fourier slice theorem. *Journal of X-ray Science and Technology*, 22(4):415–436, 2014.

- [20] S.-R. Zhao and H. Halling. A new fourier method for fan beam reconstruction. In *Nuclear Science Symposium and Medical Imaging Conference Record, 1995., 1995 IEEE*, volume 2, pages 1287–1291. IEEE, 1995.